AIAA JOURNAL
Vol. 32, No. 8, August 1994

Investigation of the Interaction of a Blast Wave with an Internal Structure

Frank Marconi*
Grumman Corporation, Bethpage, New York 11714

A computational investigation of the interaction of a blast wave with a simple internal structure is presented. The focus of the research is on the fluid dynamics involved in the explosion and the resulting shock interactions. In particular, a Rayleigh-Taylor-type instability associated with the density gradients behind the blast wave is studied in detail. Computational issues associated with the accurate prediction of this phenomenon are considered. The effects of this instability on the complex blast wave system and vice versa are fully analyzed.

Introduction

THE flowfield generated by the interaction of a blast wave with an internal structure is the subject of this investigation. The motivation behind this work stems from an interest in predicting the dynamic response of a structure to an internal explosion. The original intent of this research was to investigate the effects of structure geometry, blast intensity, and the placement of the blast center on the structure's integrity. During the early phases of the investigation, an interesting fluid dynamic phenomenon was discovered. The computational results exhibited an instability, which can be attributed to a Rayleigh-Taylor phenomenon. This paper will present an investigation of the computation of this Rayleigh-Taylor instability and its effect on the interaction of the blast wave with a simple internal structure. A similar instability has been found experimentally[1] in the case of cylindrical blast waves. In addition, analytical work in this area[2] has substantiated the instability of the contact sheet separating the detonation products from the shocked ambient gas. Computational work in the area of astrophysics[3] shows the same phenomenon.

The flow considered here is sketched in Fig. 1. An explosion is initiated at $t = x = y = 0$. After a short, complex, initial interval, the flow structure shown in Fig. 1 is developed. A strong circular shock moves into a gas at rest, imparting a radial, outward velocity on the gas particles as it passes over. The shock starts at $t = 0$ at essentially an infinite strength, and its strength decreases with increasing time. The shock decreases in strength very rapidly at the beginning of the process. The gas velocity at the origin of the blast is zero and remains so while it is undisturbed. A region of hot, low-velocity gas is left near the origin of the explosion. This region of hot gas (inside the dashed line of Fig. 1) expands slowly from the center of the explosion. It is in this region where the Rayleigh-Taylor instability first occurs.

As time progresses, the shock reflects off the walls of the structure and begins to move in toward the region of hot gas. The interaction of the shock with this region seems to set off the instability in the flow. Although this interaction is not required for the flow to exhibit the instability,[1,2] it does seem to excite the unstable modes in the flow. The interaction of the shock with this unstable, high-temperature, low-density core will be discussed in detail in the Computational Results section.

The investigation considered here is purely computational. The blast is assumed cylindrical so that the flow is two-dimensional. In this way we can use computational grids that allow us to control issues associated with numerical dissipation. It is further assumed that the flow is ideal and inviscid. The products of the explosion remain very near its origin and can be neglected.[4] The resulting model is the fully nonlinear Euler equations for an ideal gas.

The flowfield which results, even with these simplifying assumptions, is dominated by a complex interacting shock system. The interaction of the shock and the hot gas core seems to set off the Rayleigh-Taylor instability of the core. The instability is such that all symmetry in the flow is lost and an essentially chaotic state is reached. It is critical to use very fine grids in these computations; first, in order to resolve the fine structures in the flow and, second, to avoid adding so much numerical dissipation that the flow is erroneously stabilized.

We first give some details of the computational procedures used, followed by the computational results. Finally, we summarize the findings of the research.

Computational Procedure

Before the intersection of the cylindrical shock and the rigid walls of the structure, the flow is essentially one-dimensional[4] and is governed by a momentum equation,

$$\frac{Dq}{Dt} = -\frac{1}{\rho}\frac{\partial p}{\partial r} \tag{1}$$

a continuity equation,

$$\frac{D\rho}{Dt} = -\rho\left(\frac{\partial q}{\partial r} + \frac{\alpha q}{r}\right) \tag{2}$$

and an energy equation,

$$\frac{DS}{Dt} = 0 \tag{3}$$

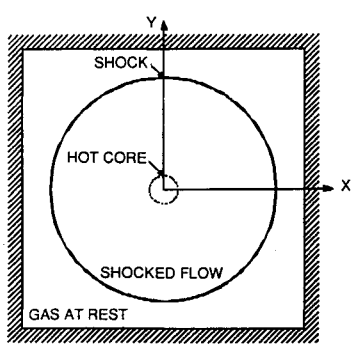

Fig. 1 Sketch of flow structure.

Presented as Paper 93-3085 at the AIAA 23th Fluid Dynamics, Plasmadynamics, and Lasers Conference, Orlando, FL, July 6-9, 1993; received Aug. 31, 1993; revision received Feb. 8, 1994; accepted for publication Feb. 19, 1994.

*Principal Staff Scientist, Research and Development Center, Aerospace and Electronics Group. Associate Fellow AIAA.

In this set of equations, r is the radial coordinate from $x = y = 0$ (Fig. 1), q is the radial velocity component, and ρ, p, and S are the density, pressure, and entropy, respectively. In the case of the cylindrical flows considered here, $\alpha = 1$ in Eq. (2). This set of equations is supplemented with an ideal gas equation of state.

This one-dimensional system was solved with Moretti's[5] upwind λ scheme.[5] The flow involves one shock running into a gas at rest. The shock was fit, resulting in a very accurate description of the flow. The forcing term $\alpha q/r$ in Eq. (2) results in a large variation in ρ, p, and q from the shock to the origin of the blast. The one-dimensional flow computation was started by assuming an arbitrarily strong shock (shock Mach number of 100). The pressure and density were assumed constant at their shock values in a small region between the shock and the blast origin. The radial velocity q was linearly decreased from the shock value to zero at the origin. The one-dimensional calculation was continued until an essentially self-similar state was reached. After an initial startup period, all independent variables (normalized to their shock values) approach a self-similar variation between the origin and the shock (with the radial coordinate r normalized to the shock position). The self-similarity is a classical result, and details of its derivation can be found in Ref. 4. Here the self-similar profiles in density, pressure, and velocity are shown in Figs. 2a–2c. Note the hot gas core of very low density and finite pressure near the origin of the blast. This region is expanding slowly with the local gas velocity as time goes on. The profiles of Fig. 2 were used as initial conditions for the fully two-dimensional flow investigated in this study. In all the cases considered here, the shock Mach number was taken as 10 when the two-dimensional flow computation was started. This corresponds to a shock pressure ratio of 116.5.

The two-dimensional computational procedure used in this investigation is based on the flux difference splitting scheme of Roe.[6] The spatial differences are second-order accurate and fully upwind. All shocks are captured with pre- and post-shock oscillations controlled with the limiter developed by van Albada et al.[7] The limiter is evaluated at every step of the calculation based on the pressure gradients. The result is that the spatial derivatives are second-order accurate everywhere but in a band very close to the shocks. All shocks are captured very sharply with this scheme (i.e., 4–5 mesh intervals). The sheer number of shocks and reflections requires very fine grids to resolve all the relevant features of the flow. These features are intimately related to the shocks, their reflections, and their interaction with the hot gas core. The possibility of adapting the grid to the shocks was considered but, because of the complexity of the interacting shock system, it was quickly realized that grid adaptation is nearly hopeless. An efficient second-order time integration scheme is used in conjunction with Roe's flux difference splitting and a simple Cartesian fine grid to produce reliable computational results. The complexity of the shock system alluded to here will become clear later in the presentation of computational results.

As the implementation of the Roe flux splitting is very similar to that presented in Ref. 8, a detailed description of the formulation of spatial derivatives will be omitted here. All computations presented use the fully second-order time-marching scheme due to Beam and Warming,[9] which will be outlined here. First consider the split-flux Euler equations in Cartesian coordinates:

$$\frac{\partial \boldsymbol{Q}}{\partial t} + \frac{\partial (E^+ + E^-)}{\partial x} + \frac{\partial (F^+ + F^-)}{\partial y} = 0 \tag{4}$$

where $\boldsymbol{Q}$ is the solution vector $\{\rho, \rho u, \rho v, e\}$, E^{+-} are the split contributions to the flux vector $\{\rho u, \rho u^2 + p, \rho vu, u(e+p)\}$, and F^{+-} are the contributions to $\{\rho v, \rho vu, \rho v^2 + p, v(e+p)\}$. The form of the splitting is again due to Roe.[6] The velocity components u and v are in the x and y directions, respectively, and e is the internal energy. A second-order expression for updating the solution vector $\boldsymbol{Q}$ can be written as:

$$\Delta \boldsymbol{Q}^k - \Delta \boldsymbol{Q}^{k-1}/(\lambda^2 - 1) - \Delta t^k \lambda/(\lambda + 1)\,(\partial \boldsymbol{Q}/\partial t)^{k+1} = 0 \tag{5}$$

where $\Delta \boldsymbol{Q}^k$ is $(\boldsymbol{Q}^{k+1} - \boldsymbol{Q}^k)$, λ is $(1 + \Delta t^{k-1}/\Delta t^k)$, and $(\partial \boldsymbol{Q}/\partial t)^{k+1}$ is evaluated from Eq. (4). Here k is the index in time. After linearization, the flux vectors $\boldsymbol{E}^{k+1}$ and $\boldsymbol{F}^{k+1}$ can be written as $\boldsymbol{E}^k + \boldsymbol{A}^k \Delta \boldsymbol{Q}^k$ and $\boldsymbol{F}^k + \boldsymbol{B}^k \Delta \boldsymbol{Q}^k$, respectively, where $\boldsymbol{A}$ and $\boldsymbol{B}$ are the flux Jacobian matrices $\partial E/\partial \boldsymbol{Q}$ and $\partial F/\partial \boldsymbol{Q}$ and are also split into positive and negative parts. The finite difference expression used to update the solution vector $\boldsymbol{Q}$ is obtained after substitution and factorization:

$$[\boldsymbol{I}/(\alpha \Delta t) + \delta_{1x}^+ \boldsymbol{A}^- + \delta_{1x}^- \boldsymbol{A}^-]$$
$$\times [\boldsymbol{I}/(\alpha \Delta t) + \delta_{1y}^+ \boldsymbol{B}^- + \delta_{1y}^- \boldsymbol{B}^-]\, \Delta \boldsymbol{Q} = \mathbf{Res} \tag{6}$$

The factorization error does not reduce the accuracy of the scheme below second order. In Eq. (6) the superscript k has been dropped, and all quantities are evaluated at the current time step. The matrix $\boldsymbol{I}$ is the identity matrix and the parameter $\alpha = \lambda/(\lambda + 1)$. δ_{1xy}^{+-} are the first-order forward and backward difference operators in the x and y directions. The use of first-order differences in Eq. (6) does not change the second-order accuracy of the overall scheme. The vector

$$\mathbf{Res} = \Delta \boldsymbol{Q}^{k-1}/[(\lambda^2 - 1)(\alpha \Delta t)^2]$$
$$- (\delta_{2x}^+ \boldsymbol{E}^- + \delta_{2x}^- \boldsymbol{E}^+ + \delta_{2y}^+ \boldsymbol{F}^- + \delta_{2y}^- \boldsymbol{F}^+) \tag{7}$$

where the difference operators δ_{2xy}^{+-} are second order. The resulting time integration scheme is second order in time and space except in small regions near shocks. The two implicit

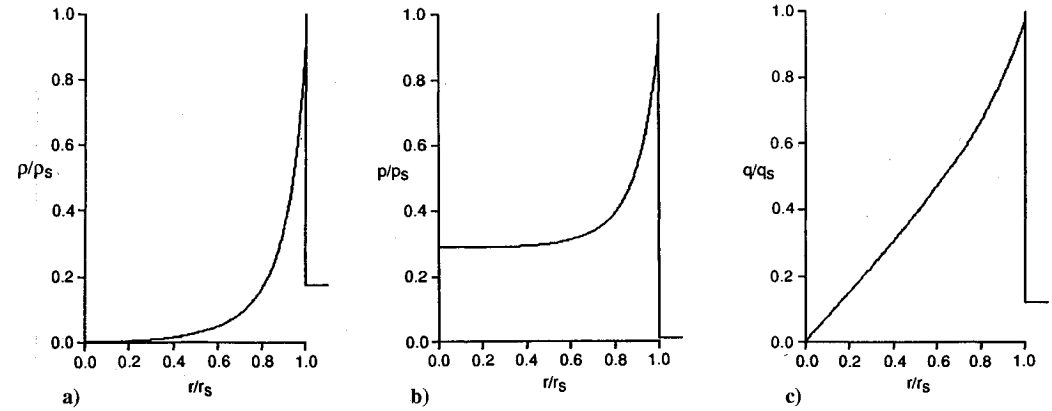

Fig. 2 Initial conditions (one-dimensional flow): a) density, b) pressure, and c) velocity.

factors of Eq. (6) result in independent tridiagonal systems in the x and y directions, which are solved in a straightforward manner.

The resulting scheme is a factored, alternating, directional implicit scheme which has been proven to be stable for time steps 40 times that of an equivalent explicit scheme for the current complex flowfields. With this scheme a pressure equilibrium state can be reached in only 1500 computational steps for the flows considered thus far in this investigation. With the fine, simple Cartesian grids used thus far (300 × 300 nodes), these computations take about 1 h of Cray Y-MP time (one processor).

Fig. 3 Density [$\ell n(\rho)$] contours computed on 300 × 300 grid; initial conditions, Mach 10 shock at center of a square room; nondimensional time interval between frames is 0.15.

Computational Results

The Rayleigh-Taylor instability in the flow considered here is caused by the fact that the net acceleration of the gas particles is directed from the lighter to the heavier gas. A detailed description of the instability can be found in Ref. 10. The one-dimensional self-similar flow sketched in Fig. 1 with the density and velocity distribution shown in Figs. 2a and 2c does indeed exhibit features consistent with a Rayleigh-Taylor instability. The gas is accelerating from the center of the explosion outward and the density is increasing in the same direction. The conditions for this instability exist from the outset of the explosion, as first discussed in the work of Refs. 1 and 2. It seems that the shock reflections promote the instability. Figure 3 shows computed density contours [more specifically $\ell n\ (\rho)$, with the density referenced to its undisturbed state] for the case started, with a Mach 10 shock intersecting the walls of a square room. The figure shows the density contours at a number of time steps during the computation. The nondimensional time increment between the time steps shown in Fig. 3 is 0.15 (where the reference time is l/a_o, l is the initial radius of the shock, and a_o is the speed of sound in the undisturbed gas). It should be noted that for 2.4 × 2.4-m (8 × 8-ft) square room at sea level, this corresponds to a time increment of about half a millisecond. In the figure, time increases from left to right, then from top to bottom. The first frame of Fig. 3 corresponds to the initial conditions in the computation (i.e., when the shock first hits the walls). The flow conditions are axisymmetric and made up of the one-dimensional profiles of Fig. 2 on each ray from the center of the explosion to the shock.

The density contours of Fig. 3 become complex very quickly due to the multiple reflections of the shock from the walls of the room. The flow should maintain quarter plane symmetry as the initial and boundary conditions are symmetric about the diagonals of the square. The computational scheme used here introduces a truncation error which destroys this quarter plane symmetry from the beginning of the computation. It is large enough to be visible in the fourth frame shown in Fig. 3 (i.e., in 1.5 ms). This error is consistent with the second-order accuracy of the scheme and is introduced in the factorization error incurred in developing Eq. (6). It can be eliminated by using a direct implicit solver for Eq. (5) or an explicit time-marching scheme. Either approach was felt to be much less efficient than the one used here. The up/down and right/left sweeps of the two factors of Eq. (6) do not introduce any up/down or right/left asymmetries. Therefore, in the calculation shown in Fig. 3, the up/down and right/left symmetry is maintained to within machine zero at the beginning of the calculation. These symmetries are lost in the results of Fig. 3 by the twelfth frame shown. By the end of the sequence shown in Fig. 3, the density contours show no symmetry at all. It is assumed here that the loss of up/down and right/left symmetry is the result of the Rayleigh-Taylor instability and is considered a symptom of that instability. The current author[11] found a similar phenomenon which resulted in asymmetric inviscid flow about cones at high angle of attack. This was due to vortex interaction. Close examination of the first dozen frames of Fig. 3 indicates the development of a number of vortices in the flow. This phenomenon is consistent with a Rayleigh-Taylor-type instability (see Refs. 1–3, and 10). At the end of the sequence shown in Fig. 3, the density contours show the flow to be somewhat chaotic, again consistent with an unstable flow.

Figure 4 shows the initial development of the flow shown in Fig. 3 in more detail. Here the nondimensional time increment is 0.015 (i.e., 0.05 ms). The first four frames show the shock segments reflecting from the four walls and moving back toward the hot gas core at the center of the explosion. The fifth frame is at a time when the region between the reflected shocks is very thin. The sixth frame shows the shocks moving away from each other. Four corner shocks (note the maximum in density at the corners) start moving toward the center in the

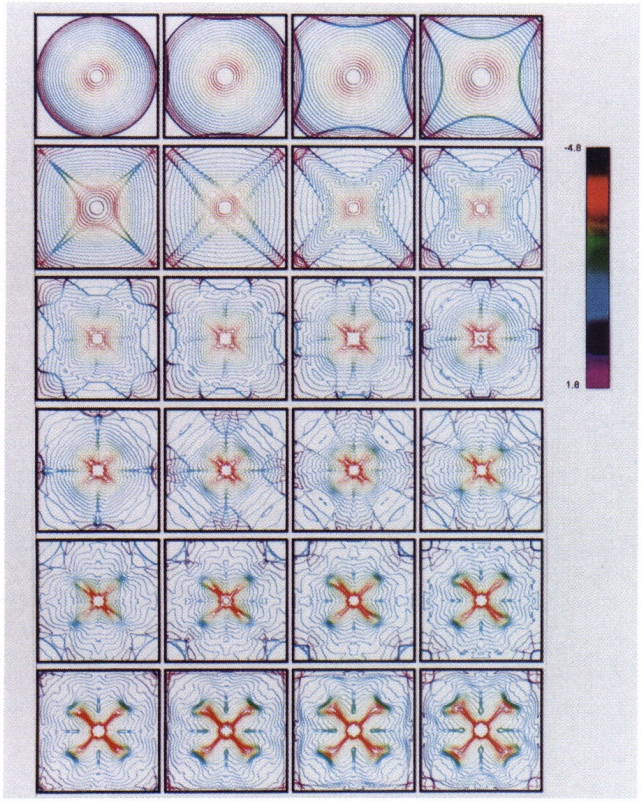

Fig. 4 Density [$\ln(\rho)$] contours computed on 300 × 300 grid; initial conditions, Mach 10 shock at center of a square room; nondimensional time interval between frames is 0.015.

fourth and fifth frames of Fig. 4. The corner shocks are substantial and quite clear in the eighth frame. The shock reflections are difficult to follow in terms of the density contours of Fig. 4 after this stage (frame 9 and above). The pressure is a better quantity for a shock system study. The pressure field of this flow will be discussed later in this paper. The deformation of the hot core is quite clear in the density contours of Fig. 4. The core, which starts out as circular, is deformed to a square shape after the first shock reflection (frame 6 of Fig. 4). The sides of this square seem to collapse and become concave in frame 9. The sides continue to collapse until the hot core has a small center connected to four lobes by thin sheets (see frame 20 of Fig. 4). The lobes at the end of the sheets roll up into vortices, and it is these vortices which signal the beginning of the development of the Rayleigh-Taylor phenomenon.

It was found in Ref. 12 that the type of instability which results in asymmetric flow about a slender body at high angle of attack is affected substantially by numerical dissipation. The calculations of Figs. 3 and 4 were done on a 300 × 300 evenly spaced Cartesian grid. Figure 5 shows results for the same case computed with a 100 × 100 grid. The time increment between frames in Fig. 5 is the same as that of Fig. 3 so that the frames can be compared directly. The first four frames of Fig. 5 show that some of the details of the results of the shock interactions are lost with the coarse grid. The most interesting aspect of the comparison is that the instability does not appear in the coarse grid calculation. Note that the up/down and left/right symmetry is preserved for the whole time sequence shown in Fig. 5. There does seem to be development of a vortex pattern in the coarse grid results, but the instability due to their interaction is missed. The numerical dissipation is so large in the 100 × 100 calculation that the physically unstable flow is erroneously stabilized. Grids finer than 300 × 300 were studied (for short time sequences), with the conclusion that the 300 × 300 grid was adequate to resolve all the important flow features.

The pressure distribution for the case shown in Fig. 3 is shown in Fig. 6. Figure 6 shows a color map corresponding to $\ln(p)$ where p is the pressure normalized with respect to the undisturbed value. The hot core at the center of the explosion does not appear as clearly in the pressure map of Fig. 6 as it does in the density contours of Fig. 3. The time interval between frames in Fig. 6 is the same as that in Fig. 3. The

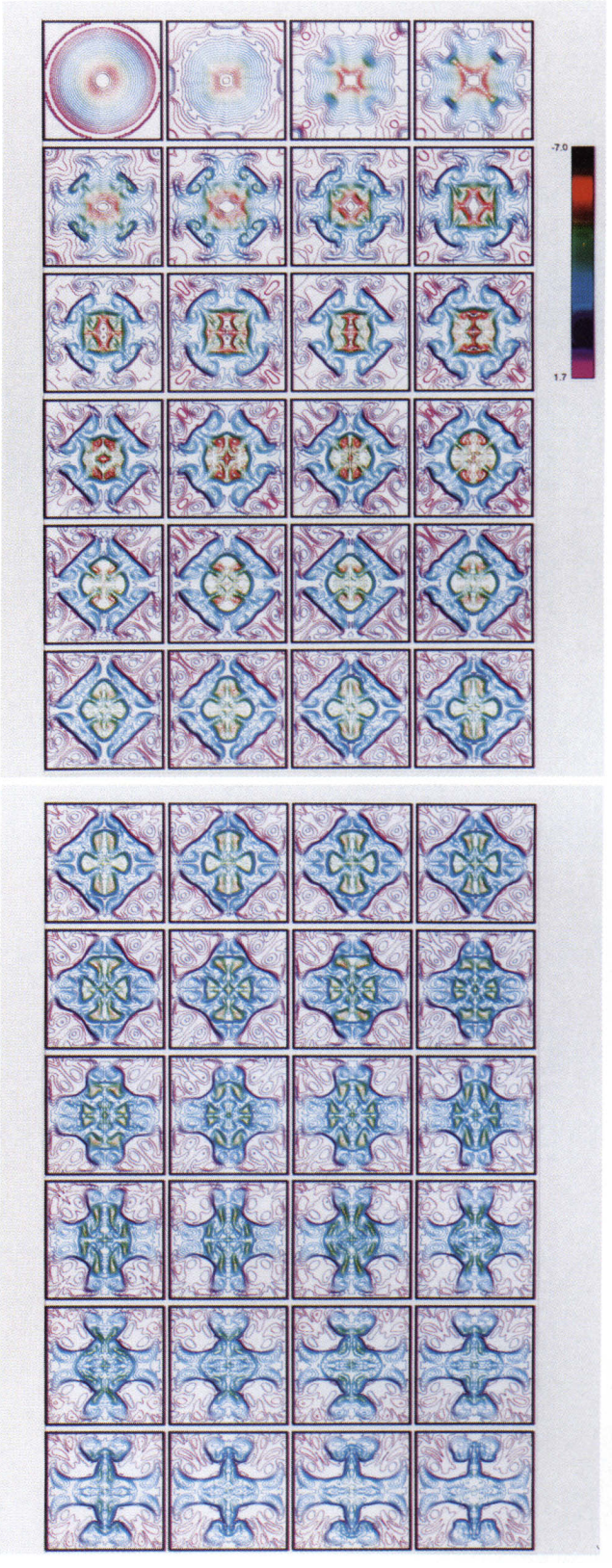

Fig. 5 Density [$\ln(\rho)$] contours computed on 100 × 100 grid; initial conditions, Mach 10 shock at center of a square room; nondimensional time interval between frames is 0.15.

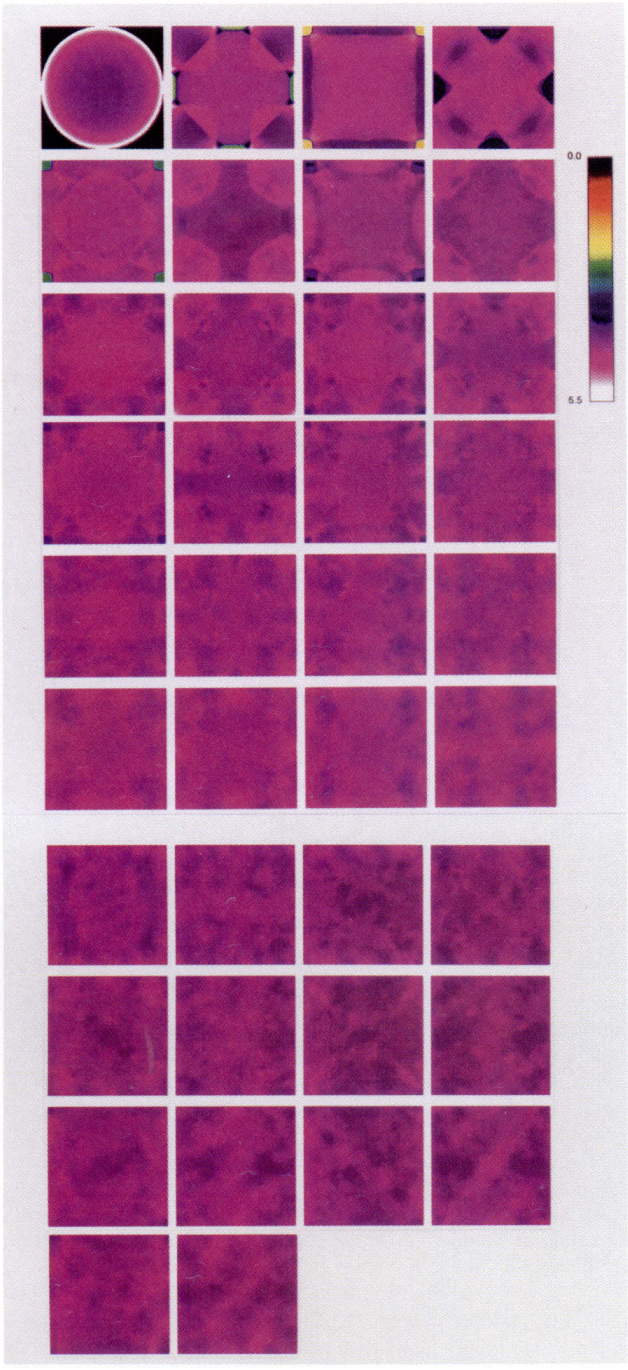

Fig. 6 Pressure [$\ell n(p)$] color maps computed on 300×300 grid; initial conditions, Mach 10 shock at center of a square room; nondimensional time interval between frames is 0.15.

shock pattern is clear in Fig. 6, and the fact that the shock system loses strength very quickly is demonstrated by the fact that the pressure essentially equilibriates 10 ms after the explosion. Figure 7 shows the isobars [lines of constant $\ell n(p)$] at the same time interval as Fig. 4 (i.e., 0.05 ms as opposed to 0.5 ms in Figs. 3 and 7). This smaller time interval between frames allows a more detailed study of the reflection of the shock system. The isobars show the shock system more clearly than the density because the frames are not cluttered with the details of the hot gas core. The first four frames of Fig. 7 show the four shock segments reflecting from the walls and moving back toward the center of the explosion. The four corner segments of the shock are still undisturbed and moving out toward their respective corners. The shock segments interact with the hot core and cross at the center of the explosion in the next four frames. In frame 9 the shock segments are moving outward toward the walls and the corner shocks are almost standing still. Note that the locations of the corner shocks in frames 10–16 are almost the same. The gas must be moving outward toward the corners and passing through a stationary shock. In this same frame the other shock segments, which now have three pieces, are moving toward the middle of the walls. Frame 9 shows this quite clearly. Note the shock segment standing off the center of the wall and parallel to it, and the two segments between this piece of shock and the intersection of the corner shock and the wall. The three-segment shock collapses at the wall center at frame 12. This interaction

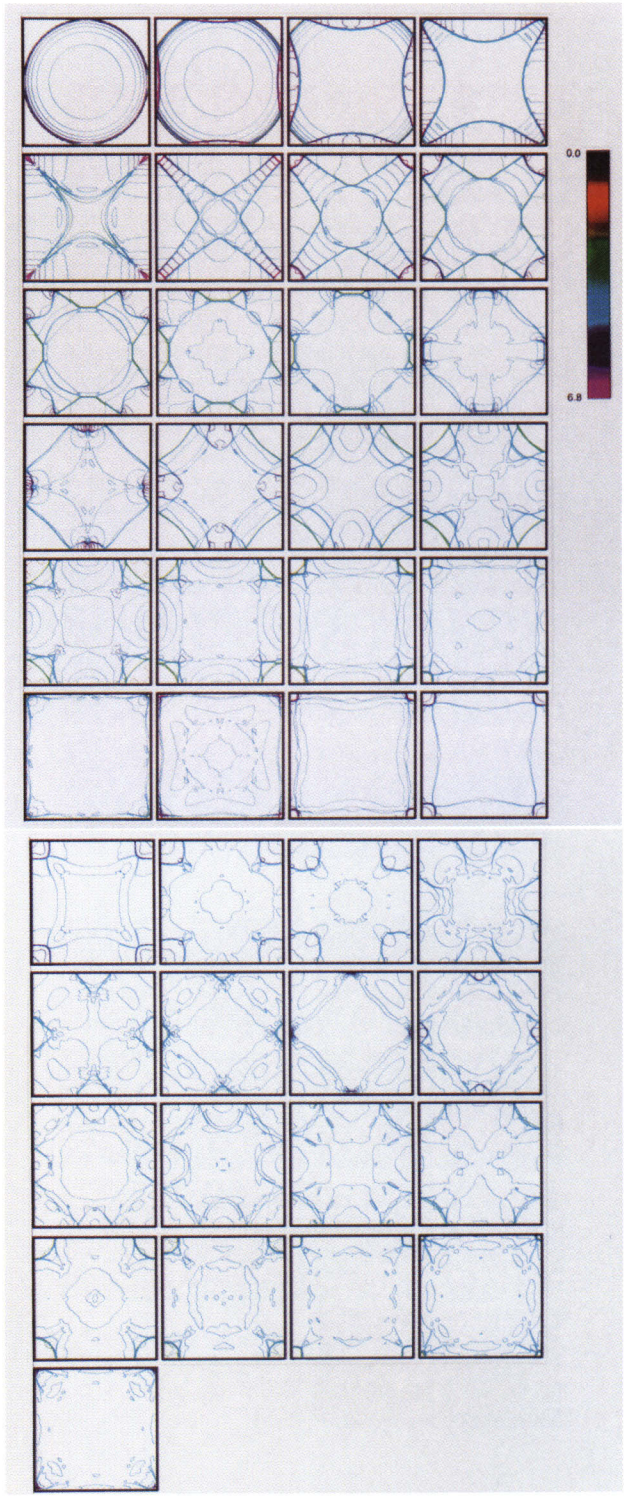

Fig. 7 Pressure [$\ell n(p)$] contours computed on 300×300 grid; initial conditions, Mach 10 shock at center of a square room; nondimensional time interval between frames is 0.015.

forms a pressure spike at the center of the wall, and another three-segment shock system is formed. One segment moves toward the explosion origin, the other two toward the adjacent corners. The spike in pressure at the corners (frame 23) is due to the arrival of these shocks.

Figure 8 shows the velocity distribution [contours of $q = (u^2 + v^2)^{1/2}$, q is nondimensionalized with respect to the undisturbed speed of sound]. Again the time increment between frames is about 0.5 ms. The velocity shows some of the same details of the hot core as shown in the density contours of Fig. 3. At the same time, the velocity approaches a uniform value (zero, a gas at rest) at large times as in the case of the pressure. In the last few frames of Fig. 8, the spots of larger

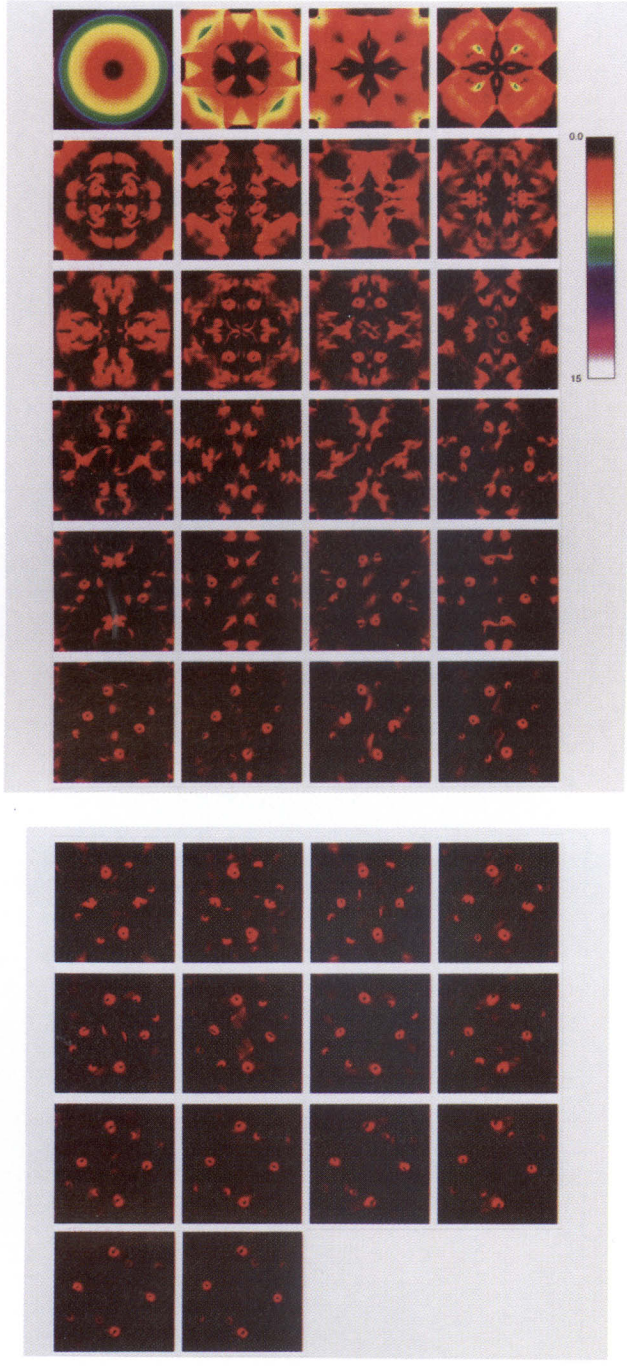

Fig. 8 Velocity $[(u^2 + v^2)^{1/2}]$ color maps computed on 300×300 grid; initial conditions, Mach 10 shock at center of a square room; nondimensional time interval between frames is 0.15.

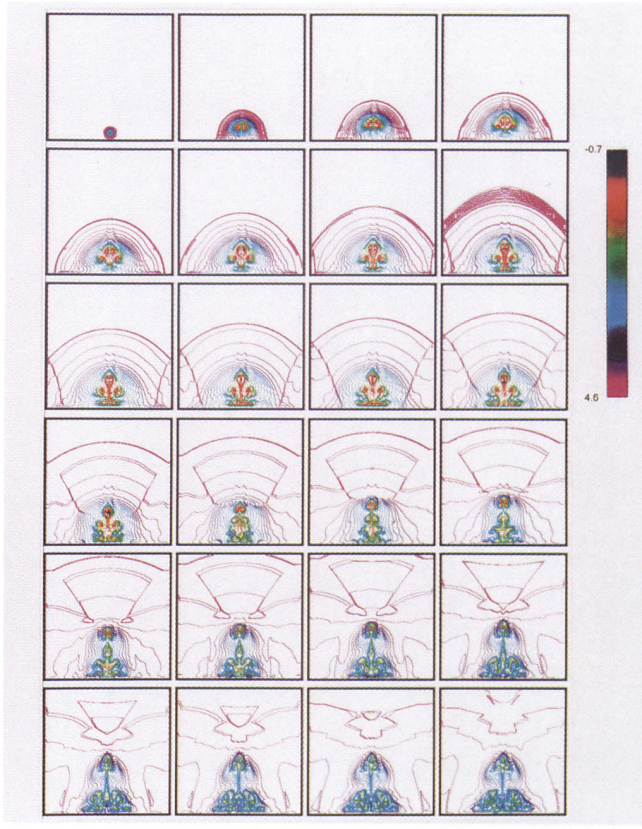

Fig. 9 Density $[\ell n(\rho)]$ contours computed on 300×300 grid; initial conditions, Mach 10 shock at the bottom of a square room; nondimensional time interval between frames is 0.6.

velocity are at the centers of the vortices left from the Rayleigh-Taylor instability.

Here is a summary of the sequence of events after the shock front reflects from the walls of a square (symmetric) room:

1) The reflected shock interacts with the low-density hot gas core exhibiting the Rayleigh-Taylor instability. The loss of flow symmetry is a result of the instability.

2) The shock system becomes very complex as it reflects from the walls and loses strength as it interacts with the expansions set up in the flow. Finally, the pressure in the room equilibrates.

3) At the end of the time sequences shown here, the room is filled with an essentially constant pressure gas. This gas is moving very slowly with the remnants of a few vortices remaining.

4) If this inviscid calculation were to be continued, it is expected that numerical viscosity would take over and dissipate any remaining flow structure.

An asymmetric geometry is shown in Fig. 9. The enclosure is still square, but this time the center of the explosion is near the floor of the room. The initial conditions for this case are shown in the first frame of Fig. 9. The center of the explosion is equidistant from the right and left walls (10 initial shock radii). The two-dimensional calculation is started when the shock first hits the floor of the room. The top of the room is 20 initial shock radii from the floor. Figure 9 shows a sequence of density contours corresponding to dimensionless time steps 0.6 apart. For an 8×8-ft room at sea level, this implies a dimensional time interval of 0.214 ms. The only symmetry that should be maintained in Fig. 9 is that about a vertical line in the center of the room. This symmetry is maintained until the tenth frame shown in Fig. 9. The Rayleigh-Taylor instability dominates the hot core of the flow, which is depicted by the blue contours in frame twenty and above. The effects of the instability have not spread over the whole flow in the time interval shown in Fig. 9. The shock reflection pattern is shown

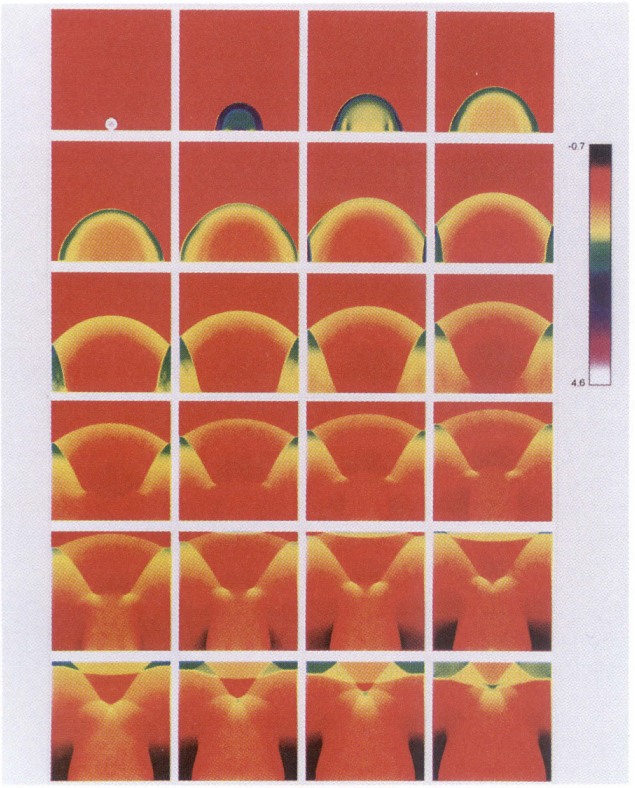

Fig. 10 Pressure [$\ell_n(p)$] color maps computed on 300 × 300 grid; initial conditions, Mach 10 shock at the bottom of a square room; nondimensional time interval between frames is 0.6.

a little more clearly in the pressure color map of Fig. 10. The shock first reflects from the floor of the room and moves up toward the hot core. This reflected shock is difficult to pick out in the first few frames of Fig. 9, but its effect on the remainder of the shock can be seen. Note how the shock differs from a semicircle in the first five frames. In frame six the shock reflects from the side walls and the reflected shock segments begin moving toward the hot core. The segments seem to accelerate near the wall as they interact with the flow gradients near the core. They cross at the center of the floor between frames 13 and 14. The essentially undisturbed upper portion of the shock hits the top wall at frame 18. The shock system is losing strength as it reflects and interacts with the expansions in the flow. Pressure equilibrium in reached at the end of the sequence shown in Fig. 10.

Summary

This investigation concentrated on the fluid dynamic aspects associated with an explosion in an enclosure. In particular, an instability in the flow associated with the Rayleigh-Taylor phenomenon was uncovered. This instability dominates the flow at the core of the explosions and can permeate the entire flow structure. While shock reflections are not required for the instability to exist, the phenomenon is linked very closely to the shock reflections from the walls of the enclosure. It was shown, quite clearly, that an accurate prediction of this flow is required to capture the instability properly. Specifically, too much numerical dissipation can erroneously stabilize the computed flowfield. It seems that the effects of the instability on the prediction of the dynamic response of a structure to an internal explosion would be significant. In addition, the phenomenon should exist in the fully three-dimensional flow. The added dimension will only make the instability more difficult to resolve. Any study which intends to uncover the effects of structure geometry, blast intensity, and/or placement on structural integrity must deal with this flow instability.

Acknowledgments

The author would like to acknowledge Howard Levine (Weidlinger Associates), Gino Moretti, and Michael Siclari and Paul Federico (Grumman Corporation) for their contributions to this work. Howard Levine provided the impetus for this work. He had hoped it would be the first step in a research program into the area of shock/internal structure interaction. Gino Moretti graciously supplied the one-dimensional initial conditions for the time-accurate two-dimensional flow computations. Michael Siclari and Paul Federico supplied and aided in the use of the software used to create all the color graphics shown in this paper.

References

[1]Davydov, A. N., Lebedev, E. F., and Perkov, S. A., "Experimental Investigation of Gas-Dynamic Instability in the Plasma Flow Following the Cylindrical Shock Wave," Preprint N1-40, Inst. of High Temperatures, USSR, 1979, p. 26.

[2]Anisimov, S. I., Zel'dovich, Y. B., Inogamov, N. A., and Ivanov, M. F., "The Taylor Instability of Contact Boundary Between Expanding Detonation Products and a Surrounding Gas," *Shock Waves, Explosions, and Detonations,* edited by J. R. Bowen, N. Manson, A. K. Oppenheim, and R. I. Soloukhin, Vol. 87, Progress in Aeronautics and Astronautics, AIAA, New York, 1983, pp. 218–227.

[3]Borrows, A., and Fryxell, B. A., "An Instability in Neutron Stars at Birth," *Science,* Vol. 258, Oct. 1992, pp. 430–434.

[4]Sakurai, A., "Blast Wave Theory," *Basic Developments in Fluid Dynamics,* edited by M. Holts, Vol. 1, Academic Press, New York, 1965, pp. 309–375.

[5]Moretti, G., "The λ-Scheme," *Computers and Fluids,* Vol. 7, No. 7, 1979, pp. 191–205.

[6]Roe, P. L., "Discrete Models for the Numerical Analysis of Time-Dependent, Multidimensional Gas Dynamics," *Journal of Computational Physics,* Vol. 63, No. 5, 1986, pp. 458–476.

[7]van Albaba, G. D., van Leer, B., and Roberts, W. W., "A Comparative Study of Computational Methods in Cosmic Gas Dynamics," *Astronomy and Astrophysics,* Vol. 108, No. 2, pp. 76–84.

[8]Thomas, J. L., Van Leer, B., and Walters, R. W., "Implicit Flux-Split Schemes for the Euler Equations," AIAA Paper No. 88-0225, Jan. 1988.

[9]Beam, R. M., and Warming, R. F., "An Implicit Finite-Difference Algorithm for Hyperbolic Systems in Conservative-Law Form," *Journal of Computational Physics,* Vol. 22, No. 5, 1976, pp. 87–110.

[10]Drazin, P. G., and Reid, W. H., *Hydrodynamic Stability,* Cambridge Univ. Press, London, 1981, p. 137.

[11]Marconi, F., "Asymmetric Separated Flows about Sharp Cones in a Supersonic Stream," *Proceedings of 11th International Conference on Numerical Methods in Fluid Dynamics* (Williamsburg, VA), June 1988, pp. 394–402.

[12]Siclari, M. J., and Marconi, F., "Computation of Navier-Stokes Solutions Exhibiting Asymmetric Vortices," *AIAA Journal,* Vol. 29, No. 1, 1991, pp. 32–42.